Non-Contact Impedance Sensing

T. Kawahara, K. Tokuda and M. Kaneko
Graduate School of Engineering
Hiroshima University
4-1, Kagamiyama 1-Chome, Higashi-Hiroshima 739-8527

Abstract

This paper discusses the non-contact impedance sensing that can measure the mass, viscosity and stiffness of environment. The developed sensor is composed of a laser displacement sensor and air force supply nozzle. We applied the developed sensor to fruits to confirm the possibility for measuring their surface impedance.

1 Introduction

There are various needs for measuring the mechanical impedance (mass, viscosity, stiffness) of environment, such as medical examination of a cancer tissue, medical examination of eye pressure, estimation of human skin age, judgment of the best time for eating fruits or meats, and evaluation of the degree of completeness of compliant material in industrial products. While various approaches have been proposed for answering these issues, most of them are based on the direct contact method [1]−[3], where the pushing force is actively given by a force probe. By the relationship between the applied force and the displacement, we can compute the impedance parameters. These approaches, however, cause several inherent issues due to the direct contact between the probe and the environment, for example, imparting damages to environment, receiving damage of the sensing probe itself, and sanitary issue especially for both foods and human beauty care.

To cope with these issues, non-contact approaches have been proposed recently and their effectiveness has been reported. As for a non-contact method, Shinoda and others [4], have first proposed the non-contact impedance sensor by utilizing air pressure actuated by an acoustic speaker, and showed the capability of measuring impedance parameters through the non-contact approach. One of most popular examples as a non-contact impedance sensor is perhaps the eye pressure measuring system [5] where air pressure is given to the eye from the front direction and the displacement of eye surface is measured by an infrared LED sensor with an inclination angle with respect to the front direction.

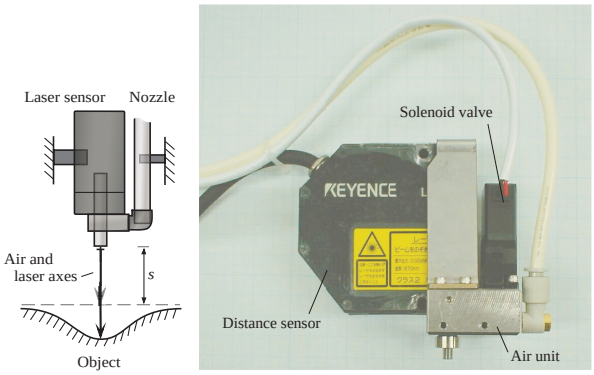

Fig. 1: An overview of the developed sensor

We discuss the non-contact impedance sensing capable of estimating the local impedance parameters without any contact. In this paper, we show the overview of the whole system including the non-contact impedance sensor[6]. As an example of application, we applied this sensor for measuring the degree of ripeness for pear. We show that impedance parameters for the pear are measured with reasonable estimation.

2 Non-Contact Impedance Sensing

2.1 Design of the Developed Sensor

Fig. 1 shows the basic design of the developed sensor unit and its overview, respectively. The sensor unit is composed of a laser distance sensor and an air supply adaptor, where s denotes the distance between the nozzle and the surface to be measured. The key idea is that the hole of air supply adaptor is so designed that the longitudinal axis perfectly coincides with the sensing axis of the laser sensor. To achieve this tuning up easily, we attach a sliding mechanism for the air

supply adaptor, which helps us to change the position with observing the laser spot. The air supply system is equipped with a high speed solenoid valve which is the key element of the sensor toward a high speed sensing. The valve can operate with the maximum switching frequency of 500[Hz] under the supply pressure of 0.05[MPa] through 0.25[MPa]. It is composed of only three mechanical components and enables us to impart a force to the environment with high response with respect to time. Such a high response allows us to estimate the impedance parameters with high quality as well as high speed. Toward a field test, we would note that since the width of air flow becomes large as s increases. This will bring both the weakness of pushing force to the environment and the low resolution of local impedance parameters in test surface. We should design the hole of the air nozzle small enough for ensuring a high resolution in surface and keep a sufficiently short s for avoiding a weak force to the environment. Another remark should be also given to the following point. Even though the axis of nozzle coincides with that of the laser sensor, it is not guaranteed that the axis of actual air flow coincides with the nozzle axis. This is because the air is supplied to the sensor unit from the side wall and largely bent with a right angle within the sensor unit. The appropriateness of design can be confirmed only through experiments.

2.2 How to Operate the Sensor

Fig. 2 shows the overview of the whole system including the non-contact impedance sensor. The system includes a compressor for producing high pressurized air source, an accumulator for keeping pressurized air, a control driver for sending the switching signal to the sensor, and a PC for collecting measured signals from the sensor as well as for sending a command signal to the driver. The command signal is produced by two parameters;

$$f_{req} = \frac{1}{\tau_{on} + \tau_{off}}, \ (0 < f_{req} \leqq 500[\mathrm{Hz}]) \qquad (1)$$

$$\alpha = \frac{\tau_{on}}{\tau_{on} + \tau_{off}}, \ (0 < \alpha \leqq 1) \qquad (2)$$

where f_{req}, α, τ_{on}, and τ_{off} are the switching frequency for the valve, the duty factor for the valuve, ON time of time period, and OFF time of time period, respectively. By changing f_{req} and α, we can produce various force patterns for each frequency.

2.3 How to Sensing Impedance

The flowchart for estimating impedance is shown in Fig. 3(a).

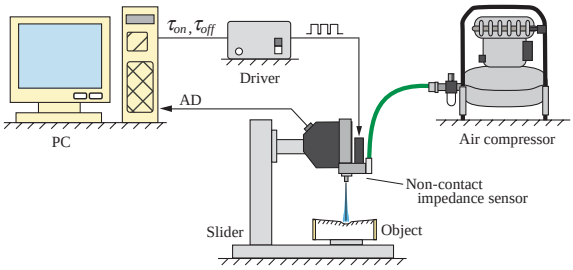

Fig. 2: Experimental system

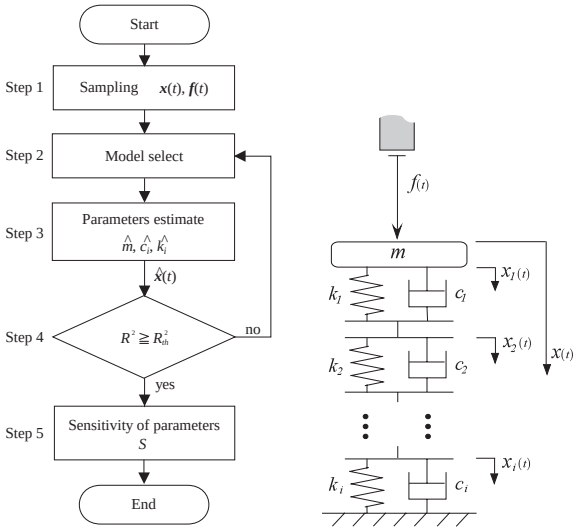

(a) Sensing flowchart (b) Impedance model

Fig. 3: Procedure for estimating impedance parameter

Step1 Measurement of the force and displacement data set:
Air force is sprayed on object and the displacement data set $\boldsymbol{x}(t) = [x_1, x_2, \cdots, x_n]^T$ is obtained. At the same time, the air force data set $\boldsymbol{f}(t) = [f_1, f_2, \cdots, f_n]^T$ is also obtained, where f_j is given step-wisely.

Step2 Select of the impedance model:
Since the behavior differs greatly from objects, the impedance model has to be carefully chosen. By considering that it generally becomes the complicated model due to the coupled spring effect, it is given by a multi-element impedance model as shown in Fig. 3(b), where m, c_i and k_i are the mass, the i-th damper, and the i-th spring, respectively.

Step3 Estimation of the model parameter:
The estimated parameters of selected model is determined by the ordinary least square method using $\boldsymbol{f}(t)$ and $\boldsymbol{x}(t)$.

Step4 Evaluation of the selected model:
The response of displacement can be reproduced by using the estimated value $\hat{m}, \hat{c}_i$ and $\hat{k}_i$. By comparing the reproduced displacement $\hat{\boldsymbol{x}}(t) = [\hat{x}_1, \hat{x}_2, \cdots, \hat{x}_n]^T$ and the actual $\boldsymbol{x}(t)$ we can evaluate how nicely the impedance are estimated. By applying the coefficient of determination R^2, we can obtain the evaluation of the degree of approximation as follows[7];

$$R^2 = 1 - \frac{\sum_{j=1}^{n} |\hat{x}_j - x_j|^2}{\sum_{j=1}^{n} |x_j - \bar{x}|^2} \qquad (0 \leqq R^2 \leqq 1) \qquad (3)$$

where $\bar{x}$ is the average value of x_j. We can say that the degree of approximation of the reproduced waveform is good, when R^2 is close to 1. If $R^2 \geqq R^2_{th}$, we progress to Step5 by regarding that the model utilized is reasonably good where R^2_{th} is the threshold value. Re-selection of a model is required when $R^2 < R^2_{th}$. We return to Step2 when $R^2 < R^2_{th}$.

Step5 Sensitivity evaluation of estimated parameters:
By Step4, We can check whether the estimated parameters are reasonable or not. However, even if R^2 becomes a large value, it is not guaranteed that the estimated parameters nicely coincide with actual ones. In order to check this, we define the sensitivity of parameter by the following[8]:

$$S = \frac{p}{g}\frac{\delta g}{\delta p} \qquad (4)$$

where g is the function of p. The sensitivity for each parameter obtained by Step3 is examined. We would note that if S is sufficiently small, the reliability of parameter estimation is not guaranteed.

3 Experiments

3.1 Air Flow Characteristics

Fig. 4 shows experimental results where Fig. 4(a), (b) and (c) are the step responses of the air jet under α=0.5, f=2.5[Hz] and s=10[mm], the air flow patterns under α=1.0 and s=10[mm], and the pushing force with respect to s under α=1, respectively. From Fig. 4(a), we can confirm that the step-up response is roughly 1[msec] while the step-down response is roughly 2[msec]. We would note that the origin of the horizontal axis in Fig. 4(b) coincides with the laser sensor axis. From Fig. 4(b), we can see a symmetry shape of the flow pattern with respect to the laser sensor axis. Now, let us define w by the width of the air pressure distribution with more than 80% of the maximum pressure. From Fig. 4(b), we can also see w=2.5[mm] for the diameter of nozzle of 2[mm], which means that the width of air flow is not big enough under s=10[mm]. In Fig. 4(c), circles and triangles show the pushing force to the environment and w, respectively. Fig. 4(c) says that the total force keeps almost constant with respect to s, while w increases gradually with respect to s. In other words, although the area affected by the air jet increases with respect to s, the pushing force does not change largely. This is because the force obtained by the integration of local pressure distribution is determined by the change of the total momentum of the air flow. The reason why the force decreases when s becomes small is that the pressurized air is difficult to come out from the nozzle due to a large flow resistance when the nozzle hole is close to the environment.

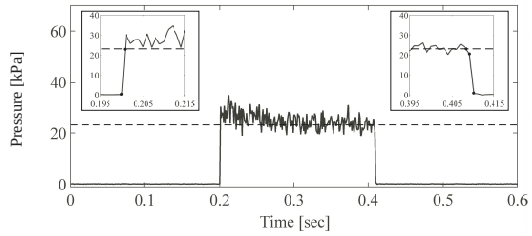

(a) Step response

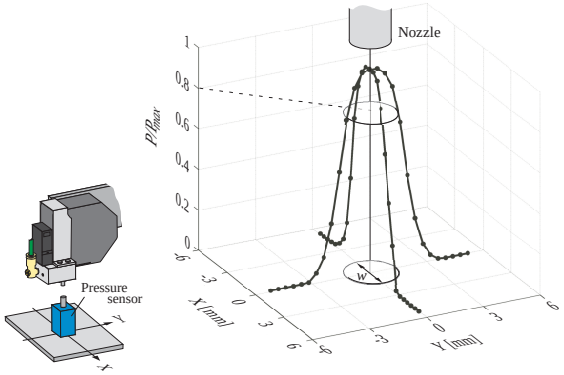

(b) Pressure distribution

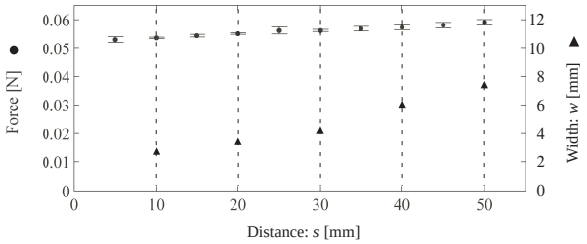

(c) Force with respect to distance

Fig. 4: Characteristics of air flow

3.2 Application to Fruit

As an example of application, we applied the developed sensor to estimate impedance parameters for pear. Fig. 5 shows the experimental result for pear. We apply stepwise air jet for 200[msec] for the surface of pear and measure the displacement of the surface. The real line in the figure shows the displacement. Although the displacement of a pear is only 60[μm], we can measure such a tiny displacement. Let us suppose that we apply a force for a linear four elements model ($i = 2$ and $m = 0$ in Fig. 3(b)). We can describe the equation of motion for the model as follows:

$$b_2\ddot{x}(t) + b_1\dot{x}(t) + b_0 x(t) = a_1\dot{f}(t) + f(t) \qquad (5)$$

$$\left(\begin{array}{ll} b_2 = \frac{c_1 c_2}{k_1+k_2}, & b_1 = \frac{c_1 k_2 + c_2 k_1}{k_1+k_2} \\ b_0 = \frac{k_1 k_2}{k_1+k_2}, & a_1 = \frac{c_1+c_2}{k_1+k_2} \end{array} \right)$$

This model is conventionally well known that it approximates the action of viscoelasticity, such as food and human skin. By using this model, we estimate $\hat{k}_1$, $\hat{k}_2$, $\hat{c}_1$, and $\hat{c}_2$, as indicated in Fig. 5. The displacement reproduced by these parameters is also expressed with the dashed line in Fig. 5. In this case, R^2 is higher than the given $R^2_{th}(= 0.950)$. Fig. 6 shows the computed sensitivity S between 100[msec] and 300[msec] in Fig. 5. From these results, $|S|_{k_1}$ is even larger than $|S|_{k_2}$, $|S|_{c_1}$ and $|S|_{c_2}$. Furthermore, we pay our attention to a time history of the sensitivity of $|S|_{c_1}$. Fig. 6 means that the parameter c_1 contributes to the response at the initial phase, for example up to 20[msec]. From the viewpoint of good estimation of c_1, we should choose the time interval in the range of 20[msec]. On the other hand, we need an appropriate time interval for obtaining sufficient number of data for estimation. There exists a compromise time interval for satisfying both requirements. We have done this experiment every two days for five pears. Fig. 7 shows the change of $\hat{k}_1$ of the pear. Through this experiment, we observe how stiffness changes every two days. In six days after we start this experiment, stiffness is changes as shown in Fig. 7. We found that the taste becomes good after six days we start this experiment. We can say this surface stiffness provides us with a good hint for judging the time for eating.

4 Concluding Remarks

We discussed the developed non-contact impedance sensor capable of estimating the local impedance parameters without any contact. We precisely explained the sensing method. As an application example, we took pear and showed that impedance parameters can be nicely evaluated by utilizing the four-elements impedance model.

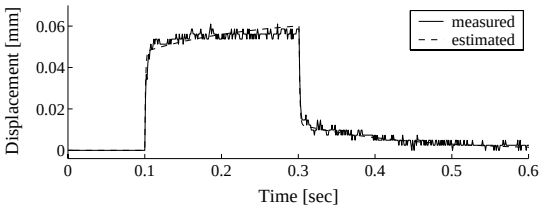

$\hat{k}_1 = 3800$[N/m], $\hat{k}_2 = 11100$[N/m], $\hat{c}_1 = 3.68$[Ns/m], $\hat{c}_2 = 1550$[Ns/m]

Fig. 5: Application to pear ($R^2 = 0.993$)

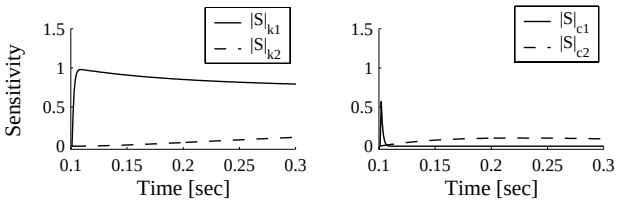

Fig. 6: Sensitivity of the eatimated parameters

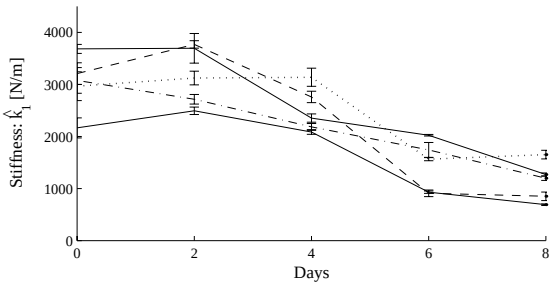

Fig. 7: Time history of stiffness of pear

References

[1] S. Omata and Y. Terunuma, "New tactile sensor like the human hand and its applications", *Sensors and Actuators A*, Vol.35, pp.9–15, 1992.

[2] Y. Yoshitoshi and M. Nagasaka, "Viscoelasetic Properties of Edematous Skin", *Japanese Heart Journal*, Vol.3, No.3, pp.220–230, 1962.

[3] H. Oka and T. Irie, "Mechanical impedance of layered tissue", *Medical Progress through Technology*, Vol.21, pp.1–4, 1997.

[4] H. Shinoda and H. Yamasaki, "Noncontact sensing of surface hardness", *J. of SICE*, Vol.27, No.7, pp.749–754, 1991.

[5] TOPCON MEDICAL SYSTEMS, INC., Non-contact tonometer, *http://www.topcon.com/medical.html*.

[6] M. Kaneko and T. Kawahara, "Co-axis type non-contact impedance sensor", *In Proc. of the IEEE Int. Conf. on Robotics and Automation*, pp.709–714, 2004.

[7] B. W. Bolch and C. J. Huang, Development of the multivariate analysis, Morikita Publishing Company, pp.133–139, 1976.

[8] K. Nonami, H. Nishimura, A foundation for the control theory, Tokyo Denki University Press, pp.94–95, 1998.